UDC621.98.042:681.3:519.6

3-D FEM Analysis of Sheet Metal Deep Drawability and Stretchability — Application of FEM Analysis to Research Formability of Sheet Metals —

Tohru Yoshida*1 Koji Hashimoto*1
Matsuo Usuda*1

Abstract:

Square cup deep drawing and hemispherical punch stretching, the optimal means of forming sheet metals, were numerically analyzed by the three-dimensional finite element method (FEM) based on the membrane theory. Methods for predicting and evaluating the formability of sheet metals and for avoiding the fracture of sheet metals were also studied. The estimation index of breakage for sheet metals in the forming processes was determined from the strain calculated by finite element method (FEM) analysis and the theoretical forming limit diagram. In the analysis of square cup deep drawing, the material properties and forming conditions were investigated for their effects on the strain path and fracture limit at weak portions such as the punch shoulder, and their quantitative relationships were clarified. In the analysis of hemispherical punch stretching, it was computationally confirmed that changing the width of square blanks changes the strain state from uniaxial tensile deformation to plane strain deformation. The effect of blank width on the limiting dome height was analyzed, and the analytical results were confirmed to agree with the experimental results in tendency.

1. Introduction

Steelmakers test the formability of newly developed materials to evaluate their service performance or to select them for specific applications. Traditionally, they carried out forming experiments with simply shaped small tools, and compensated for insufficient data by referring to past forming results. These conventional procedures produced only qualitative results and were not capable of accurately evaluating materials.

In recent years, computers have advanced in both hardware and software to the extent that they can now analyze sheet metal forming problems or nonlinear and large-deformation problems that were very difficult to solve due to the complex change in boundary conditions. With the aid of numerical analysis techniques, it appears possible to achieve the optimal forming of sheet metals by combining material properties and forming conditions in an appropriate manner.

Square cup deep drawing and hemispherical punch stretching of sheet metals, the optimal method of forming sheet metals, were numerically analyzed by the three-dimensional FEM based on the membrane theory. Methods for predicting and evaluating the formability of sheet metals and for avoiding sheet metal frac-

*1 Technical Development Bureau

ture were also studied. For square cup deep drawing, the material properties and forming conditions were analyzed for their effects on the strain path of sheet metals, and the fracture limits of sheet metals were predicted and evaluated. For hemispherical punch stretching, the limiting dome height was determined from the strain path of fractured portions and by applying localized necking theory. The analytical techniques employed were investigated for their correlation with experimental techniques.

2. Outline of Forming Simulation System

To predict and evaluate the formability of sheet metals, it is necessary not only to faithfully simulate the forming process concerned, but also to accurately predict fracture and forming limits. This can be accomplished by a practical simulation system that combines FEM analysis with fracture estimation. **Fig. 1** shows the configuration of the forming simulation system. Two to three types of three-dimensional elastic-plastic programs for the analysis of sheet metal forming are used as FEM solvers. Of such programs, ROBUST is a static explicit program using membrane elements and is advantageous in that it can solve complex contact problems without divergence. Computing time is shortened by using triangular membrane elements with single integration point at the center of gravity of each element and by achieving incremental control by the r-min method. The material model is described by an elastic-plastic constitutive equation based on Hill's anisotropic plastic yield function equation (1), the Swift-type work hardening equation (2), and a contact force constitutive equation based on Coulomb's law of friction. A data base of tensile test and sliding test results for carbon steel, high-strength steel, aluminum alloys, and stainless steel is developed to furnish material properties to be used in calculations.

$$f=(G+H)\sigma_x^2+(G+F)\sigma_y^2-2H\sigma_x\sigma_y+2N\sigma_{xy}^2=2\sigma^2 \quad \cdots(1)$$

$$\sigma=K(\varepsilon_0+\varepsilon_p)^{n^*} \quad \cdots(2)$$

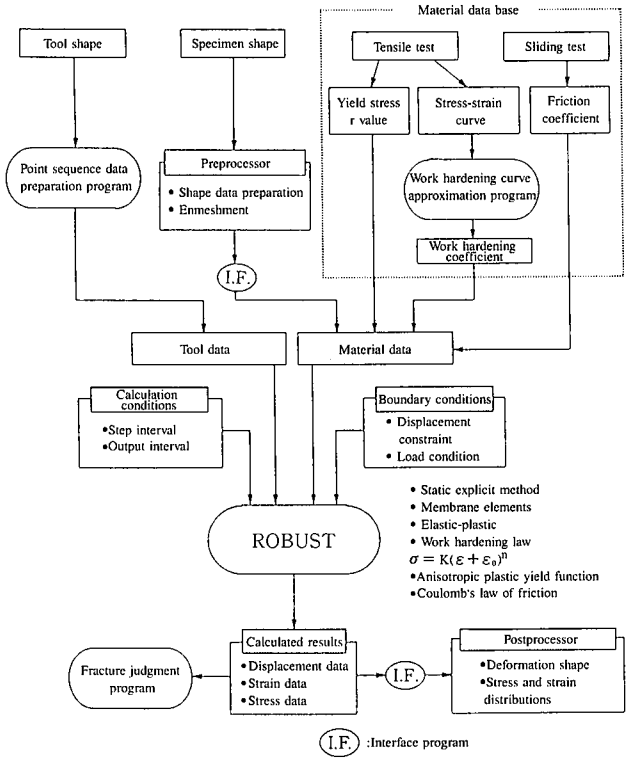

Fig. 1 Configuration of forming simulation system

3. Analytical Methods

3.1 FEM analysis of forming processes

The dimensions of square cup deep drawing tools are shown in **Fig. 2**. The blank was set so that its rolling direction was parallel to the sides of the punch. In view of its symmetry, computation was performed on a quarter of the formed part. The blank was analyzed by using a mesh composed of 1, 800 elements and 961 nodes. A blank holding force (BHF) of 30 kN was assumed to apply to the whole of the blank. Three grades of cold-rolled sheet steel of 0.8 mm thickness (SPCC, SPCE, and SPCE-N) were analyzed as to the effect of their properties on the deep drawing of square cups. To clarify the effects of material properties and forming conditions on the strain path and fracture limit, the n value, r value, BHF, friction coefficient, blank shape, and tooling geometry were used as computational parameters. The material properties and forming conditions are given in **Tables 1** and **2**, respectively.

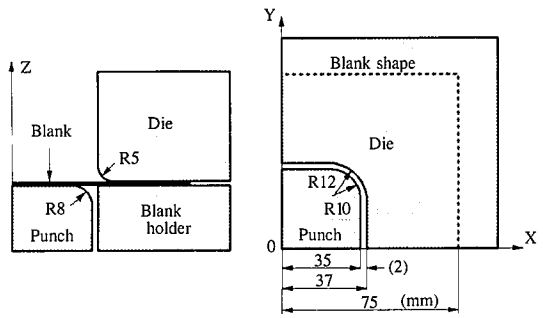

Fig. 2 Square cup deep drawing tools

Table 2 Square cup deep drawing conditions analyzed

Symbol	Blank holder force BHF (kN)	Blank shape, Corner cut Lc (mm)	Die shape, Corner shoulder radius Rc (mm)
a	19.6	0	10
b	29.4	0	10
c	39.2	0	10
d	29.4	20	10
e	29.4	40	10
f	29.4	0	15

Table 1 Material properties entered into system

Symbol	Material	YS (MPa)	TS (MPa)	T-El (%)	E (GPa)	n value 5-15%	r value 15%	Work hardening coefficient			Friction coefficient
								K(MPa)	ε_0	n*	μ
A0	SPCC	279	363	41.6	210	0.221	0.99	645	0.0093	0.238	0.130
B0	SPCE	169	318	43.3	210	0.241	1.72	586	0.0078	0.249	0.130
C0	SPCEN	126	276	54.0	210	0.296	2.41	522	0.0012	0.287	0.130
D0	SUS304	299	674	56.0	193	0.353	1.01	1269	0.0720	0.615	0.092
E0	5000 series Aluminum alloy	121	261	31.9	70	0.330	0.76	417	0.0096	0.345	0.130

Table 1 shows the properties of carbon steel SPCE, stainless steel SUS304, and 5000 series aluminum alloy, which were used to analyze hemispherical punch stretching also. The dimensions of the hemispherical punch stretching tools used are shown in **Fig. 3**. A quarter of the formed part was analyzed in the same way as done for the square cup deep drawing process. Considering that there is practically no drawing-in of the flange outside of the lock bead, the nodes at a distance of more than 82.5 mm from the center were constrained with zero displacement. The blankholder force to be applied to the flange was calculated from the contact area. Models with blank widths of 80, 100, and 140 mm were prepared and analyzed to study the effect of the blank shape on strain path and limiting dome height. The numbers of elements and nodes in the three blank sizes analyzed are given in **Table 3**.

3.2 Method for evaluating fracture limit

The major strain ε_1 of each element at a given forming height is obtained by FEM analysis. Since the fracture limit strain ε_1^* varies with the strain ratio, the fracture occurrence cannot be quantitatively evaluated from the magnitude of ε_1 alone. In this analysis, the following index is used for the quantitative evaluation of the fracture occurrence by referring to the Stören-Rice localized necking limiting strain value:

$$I_b = \varepsilon_{1a} / \varepsilon_1^*(\beta, n, \psi) \quad \cdots(3)$$

where I_b = fracture estimation index; ε_{1a} = major strain in portion a; ε_1^* = Stören-Rice localized necking limiting major strain; β = strain ratio ($= \varepsilon_2/\varepsilon_1$); ε_2 :minor strain; n = work hardening exponent (n value) of the material; and ψ = angle between the direction of the major strain and the direction normal to the necking line.

The material being press formed fractures immediately after the onset of localized necking. The use of the localized necking condition as a criterion is considered an evaluation on the safe side of the forming limit. When it is necessary to also consider ductility after the occurrence of localized necking, as is the case with stretching, the use of limiting strain under plane strain deformation as the n value can more faithfully simulate the actual fracture limit.

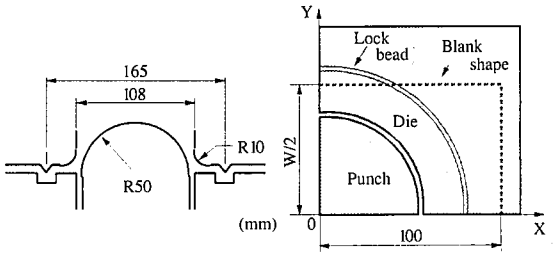

Fig. 3 Hemispherical punch stretching tools

Table 3 Enmeshment of blank shapes analyzed (hemispherical punch stretching)

Symbol	Blank width W (mm)	Number of elements	Number of nodes
I	80.0	1,056	578
II	100.0	1,320	714
III	140.0	1,848	986

4. Analytical Results and Discussion

4.1 Analysis of square cup deep drawing

4.1.1 Strain distribution and strain path

The principal strain distributions of SPCE (B0) in the diagonal direction of the square cup are shown in **Fig. 4**. Since the strain value depends on the gauge length, it was experimentally measured so that the gauge length would approach the length of the analytical elements. From **Fig. 4**, it can be seen that the strain in the forming process can be predicted with considerably high accuracy. **Fig. 5** shows the analyzed strain path sections of portions P_1 and P_2. P_1 is the portion that is likely to fracture at the punch shoulder, and its deformation proceeds in the range of

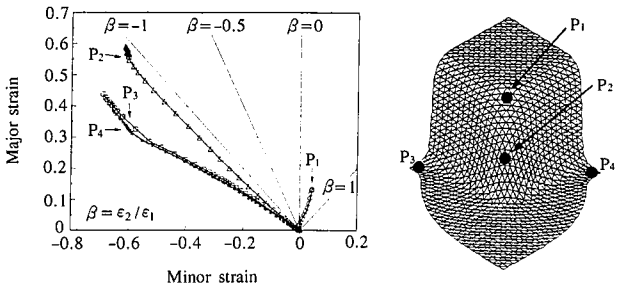

Fig. 5 Analysis of deformation shape and strain path in square cup deep drawing process

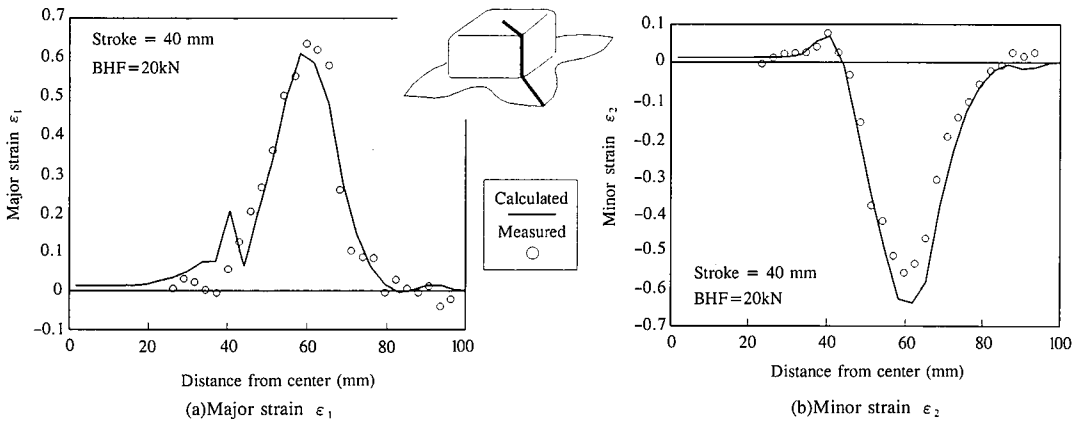

Fig. 4 Principal strain distribution in diagonal direction

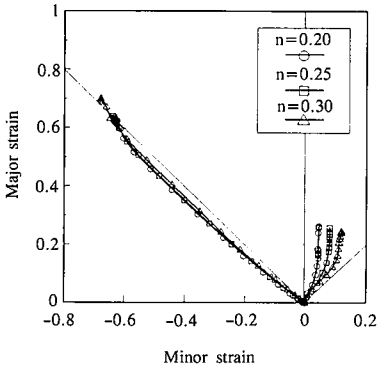

Fig. 6 Effect of n value on strain path

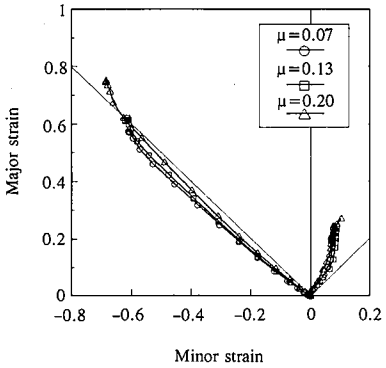

Fig. 8 Effect of friction coefficient on strain path

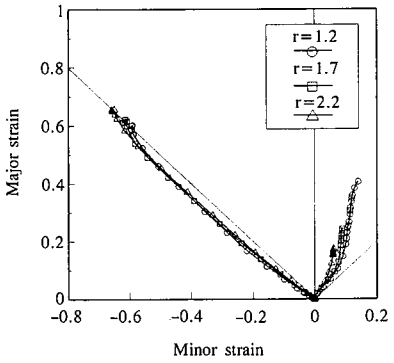

Fig. 7 Effect of r value on strain path

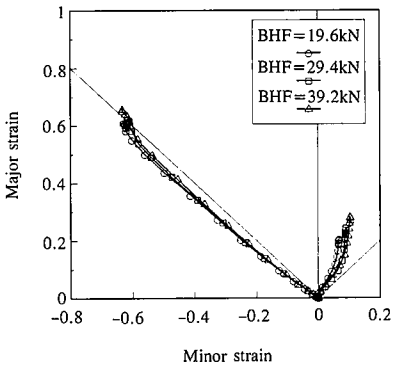

Fig. 9 Effect of BHF on strain path

plane strain deformation to biaxial deformation. P_2 is the portion that is likely experience necking in the wall, and its deformation mode is such that it is subjected first to large shear deformation in the flange and then to tensile deformation as it moves from the die shoulder to the wall. The large shear deformation of portion P_2 can also be observed from **Fig. 5**.

4.1.2 Effects of material properties and forming conditions on strain path

The effects of the material properties and forming conditions on the strain paths of portions P_1 and P_2 are shown in **Figs. 6** to **9**. The following is understood from the results of **Figs. 6** to **9**: 1) As the n value increases, the minor principal strain ε_2 increases, and the deformation mode shifts to biaxial deformation. The strain path of portion P_2 changes little, but since the drawing-in of the flange is promoted by the work hardening of the flange when the n value is large, the major strain ε_1 of portion P_2 is large. 2) When the r value increases, the strain ratio β $(= \varepsilon_2/\varepsilon_1)$ changes little at the same forming height, but the decrease in the drawing resistance of the flange increases the drawing-in of the flange and sharply reduces the major strain ε_1. The increase in the drawing-in of the flange accelerates the movement of portion P_2 into the wall and slightly increases the amount of deformation as well. 3) The effect of the friction coefficient on the strain of portion P_1 is not clear. This is probably because the BHF was low and because the strain concentration position was changed under the influence of the friction coefficient. The increase in the frictional resistance in portion P_2 decreases the drawing-in of the flange and increases the amount of deformation. 4) The effect of the BHF is pronounced in portion P_1, and the increase in the BHF shifts the deformation mode to biaxial deformation and increases the major strain ε_1.

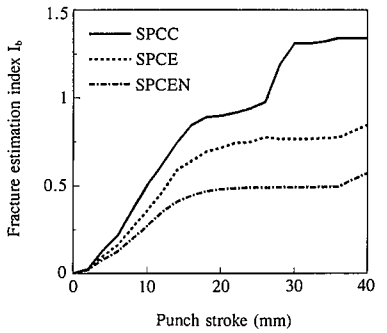

Fig. 10 Fracture estimation index of materials (calculated values)

4.1.3 Evaluation of forming limit

Since the fracture of the blank in the square cup deep drawing process mainly occurs at the punch shoulder, the fracture occurrence was evaluated with respect to the principal strain of portion P_1. According to Eq. (3), the fracture estimation index I_b equals one and the blank reaches the fracture limit when the major strain ε_1 reaches the limiting strain ε_1^*. **Fig. 10** shows the ratio of strain increase to fracture of three materials as quantified with respect to the punch stroke by using the fracture evaluation index I_b. From this figure, it is clear that the materials greatly vary in formability under the same forming conditions. The effects of the material properties and forming conditions on the fracture estimation index I_b with a forming height of 40 mm are

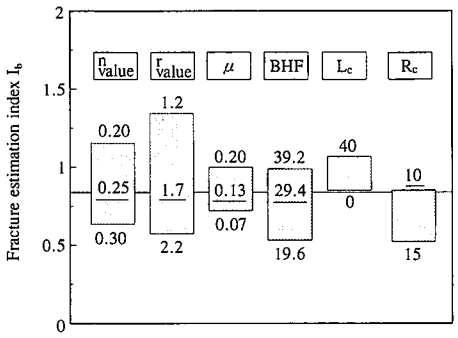

Fig. 11 Effects of material properties and forming conditions on fracture estimation index

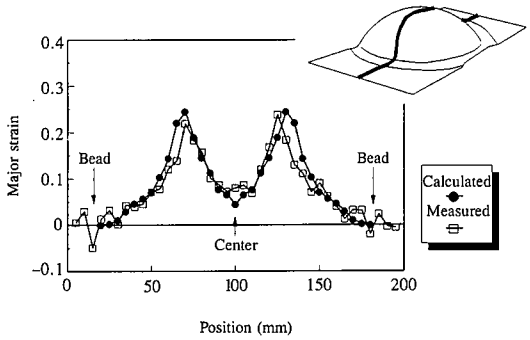

Fig. 12 Major strain distributions (SPCE, W = 140 mm)

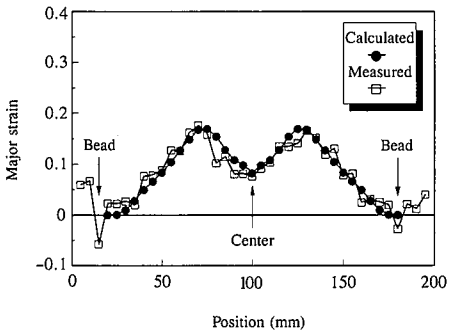

Fig. 13 Major strain distributions (SUS304, W = 140 mm)

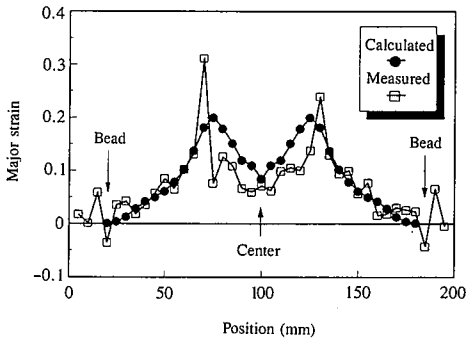

Fig. 14 Major strain distributions (5000 series aluminum alloy, W = 140 mm)

shown in **Fig. 11**. These results verify the effectiveness of the forming simulation system in quantifying the effects of various factors on the fracture phenomenon and obtaining general-purpose data to present methods for avoiding the fracture of blanks.

4.2 Analysis of hemispherical punch stretching

4.2.1 Strain distributions

The analytical and experimental principal strain distributions of SPCE (B0), SUS304 (D0), and 5000 series aluminum alloy (E0) are compared in **Figs. 12** to **14**, respectively. The gauge length was 5 mm for both of the calculated values and the measured values. The calculated strain distributions of SPCE and SUS304 approximately agree with the measured strain distributions. This means that the effects of tool-material contact conditions, including friction conditions, and material properties were analyzed with considerable accuracy. With the 5000 series aluminum alloy, however, the strain distribution where the material is in contact with the tooling was not accurately simulated. This is probably because the sliding characteristics of the aluminum alloy that is likely to gall cannot be expressed by Coulomb's law of friction, or because the decrease in the n value with the increase in the strain is not taken into account by the analysis performed.

4.2.2 Effect of blank width on strain path

The strain path of portion P_5 in **Fig. 15** was analyzed. The analytically and experimentally determined effects of the blank width on the strain path are shown in **Fig. 16**. The strain path greatly varies with blank width. The deformation mode is approximately uniaxial tensile deformation when the blank width was 80 mm and shifts to plane strain deformation as blank width increased. In this way, the calculated strain paths agreed well with the measured strain paths.

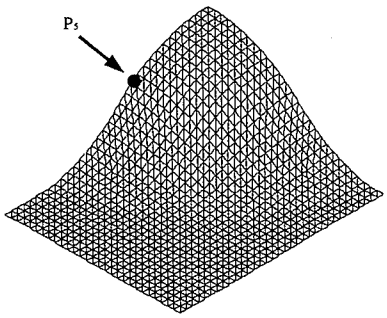

Fig. 15 Deformation shape and analytical position of strain path in analysis of hemispherical punch stretching

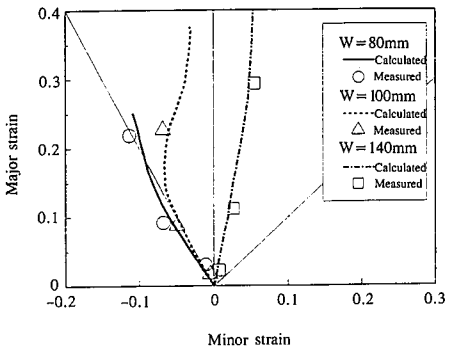

Fig. 16 Effect of blank width on strain path

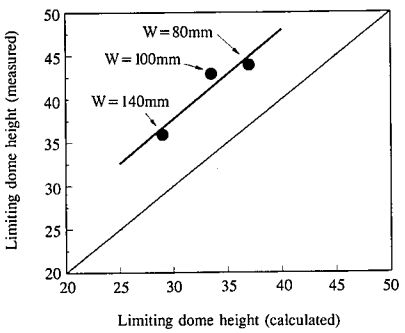

Fig. 17 Comparison of calculated and measured values of limiting dome height

4.2.3 Evaluation of limiting dome height

The forming height at which there appears an element with a fracture estimation index as expressed by Eq. (3) equals to one is defined as the limiting dome height in the forming simulation process using the FEM. The calculated and measured effects of blank width on the limiting dome height are compared in **Fig. 17**. From **Fig. 17**, it is evident that the limiting dome height increases with decreasing blank width. This was probably because the decrease in the blank width in the range analyzed here changes the deformation path of the fractured portion from deformation close to plane strain to uniaxial tensile deformation, and increases the limiting strain ε_1*. The trends of the analytical results were the same as that of the experimental results in this respect. Irrespective of blank width, however, the calculated limiting dome height was smaller than the measured limiting dome height. The limiting strain used in the analysis is based on the occurrence of localized necking. Localized elongation after the onset of localized necking was not taken into account. For this reason, the calculated fracture limit strain was perhaps smaller than the measured fracture limit strain.

5. Conclusions

Using the three-dimensional FEM based on the membrane theory, a system was developed that can predict and evaluate the formability of sheet metals. The system was used to simulate the deep drawing and stretching of sheet metals and to study the effects of material properties and blank size on the strain path. The fracture limit of sheet metals was predicted and evaluated in comparison with the theoretical forming limit diagram (FLD) for the simple loading path. In analyzing the square cup deep drawing process, the material properties and forming conditions were investigated for their effects on the strain path and fracture estimation index of blank portions highly susceptible to fracturing at the punch shoulder. Their quantitative relationships were also clarified. In analyzing the hemispherical punch stretching process, it was confirmed by both calculation and experiment that changing the width of the square blank alters the strain state from uniaxial tensile deformation to plane strain deformation. The effect of the blank width on the limiting dome height was analyzed, and the analytical results were confirmed to agree with the experimental results. A more accurate evaluation with respect to the prediction of the limiting dome height would involve, for example, forming limit diagrams that more strictly take the local deformation characteristics of specific materials into account.

References

1) Ohwue, T., et al.: Proceedings of 42nd Japanese Joint Conference for Technology of Plasticity. 1991, p.17
2) Yoshida, T., et al.: Proceedings of 43rd Japanese Joint Conference for Technology of Plasticity. 1992, p.73
3) Nakamachi, E.: Proceedings of NUMIFORM '92. 1992, p.509
4) Yoshida, T., et al.: Proceedings of NUMISHEET '93. 1993, p.219
5) Yoshida, T., et al.: Proceedings of 44th Japanese Joint Conference for Technology of Plasticity. 1993, p.265
6) Yoshida, T., et al.: 18th Biennial Congress of IDDRG. 1994, p.437
7) Hill, R.: The Mathematical Theory of Plasticity. Oxford University Press, 1950
8) Stören, S., Rice, J.R.: Journal of Mechanical Physics & Solids. 421 (1975)